Engineering Computations

Article information:

Users who downloaded this article also downloaded:

For Authors

About Emerald www.emeraldinsight.com

A yield function for granular materials based on microstructures

Sihong Liu, Zijian Wang, Yishu Wang and Liujiang Wang
*College of Water Conservancy and Hydropower Engineering,
Hohai University, Nanjing, China, and*

Zhongzhi Fu
Nanjing Hydraulic Research Institute, Nanjing, China

Abstract

Purpose – The purpose of this paper is to propose a new yield function for granular materials based on microstructures.

Design/methodology/approach – A biaxial compression test on granular materials under different stress paths is numerically simulated by distinct element method. A microstructure parameter S that considers both the arrangement of granular particles and the inter-particle contact forces is proposed. The evolution of the microstructure parameter S under the simulated stress paths is analyzed, from which a yield function for granular materials is derived. The way of determining the two parameters involved in the yield function is proposed.

Findings – The new yield function is calibrated using the test data of one sand and two rockfill materials. The shape of the new yield surface is similar to that of the Cam-clay model.

Originality/value – The paper proposes a microstructure parameter S, which considers both the arrangement of granular particles and the inter-particle contact forces. From the evolution of S, a yield function for granular materials is derived. The proposed yield function has a simple structure and the parameters are easy to be determined, leading to a feasible realization of engineering application.

Keywords Microstructure, Granular material, DEM, Stress path, Yield function

Paper type Research paper

1. Introduction

A yield function is one of the cores in classic elasto-plastic theories, which is the criterion of loading and unloading. The corresponding yield surface is the boundary to distinguish the elastic deformation region and the plastic deformation region. A number of yield functions have been proposed for geo-materials. The earliest one may be the Mohr-Coulomb rule, which was developed by Mohr in 1900 from the Coulomb's rock failure criterion. Roscoe *et al.* established a yield function on the basis of drained and undrained triaxial compression tests on normally consolidated and overconsolidated clay, from which the famous Cam-clay model was developed. It is the earliest classic elasto-plastic constitutive model of soils that can better reflect the elasto-plastic deformation characteristics of soils, especially the plastic volumetric deformation (Roscoe *et al.*, 1958). Another yield functions that are the most commonly used may be the Drucker-Prager, Matsuoka-Nakai and Lade-Duncan criteria (Drucker *et al.*, 1955; Lade and Duncan, 1977; Matsuoka *et al.*, 1999). These yield functions were

established mostly on the basis of macroscopic experiments or on the assumption of the energy dissipation. Few attentions were paid on the microscopic essence of yield functions.

Granular materials consist of discrete particles and their mechanical properties depend largely on the linkage and arrangement of particles that are defined as the microstructures. Now, the study of the microstructures of granular materials is a hot issue. As early as the 1920s, Terzaghi, the founder of Soil Mechanics, first, suggested the honeycomb structure of clay, starting the research on the microstructure of soils. In the past decades, great efforts have been devoted to study the macroscopic mechanics behavior of granular materials in terms of its microstructures. For example, Oda (1972) studied the particle contact normals of sand samples after triaxial compression tests, and found that the frequency distribution of particle contact normals concentrates on the direction of the major principle stress during shearing (Oda, 1972); Matsuoka (1974) carried out direct shear tests on assemblies of both photoelastic and aluminum rods, on which a stress-shear dilatancy equation was derived from the frequency distribution of particle contacts on the mobilized plane (Matsuoka, 1974).

As granular materials consist of particles, it is more realistic to study their mechanical behaviors if we use distinct element approaches in which the particle arrangement is modeled explicitly. Recent distinct element approaches started with the distinct element method (DEM) that was first developed by Cundall for rock mass problems and later applied to granular materials by Cundall and Strack (1979). DEM can provide sufficient micro-mechanical data such as the displacement of individual particles, contact orientations, contact forces and mobilized inter-particle frictional angles. It is based on the Newton's Second Law of Motion, and does not need constitutive models as used in continuum approaches, which are gotten from experiments or experiences. Thus, DEM is especially fit for studying the mechanism of granular materials. For example, it has been applied to study the stress-dilatancy relation (Liu and Matsuoka, 2003; Liu, 2006), wetting-induced collapse mechanism (Liu and Sun, 2002; Liu et al., 2003) and slope failure mechanism (Chen and Liu, 2007; Liu and Bauer, 2007) of granular soils. Discrete element simulation has already become an effective method and also an important supplement of laboratory experiments in the study of mechanical properties of granular materials.

In this paper, a biaxial compression test on granular materials under different loading stress paths is numerically simulated by DEM, and a parameter that characterizes the microstructures of the numerical samples is proposed. The evolution of the proposed microstructure parameter during loading is then investigated, from which a new yield function for granular materials is derived. The calibration for the new yield function is carried out and the determination of the two parameters involved in the new yield function is studied.

2. Discrete modeling of biaxial shearing test
The DEM is a numerical technique in which individual particles are represented as rigid bodies. It provides a valuable tool to obtain quantitative information of all microscopic features of an assembly of particles. In two dimensions each particle has three degrees of freedom (two translations and one rotation). Each particle can be in contact with neighboring particles or boundaries. In the present work, the particles used in the numerical simulation are circular because of their simple shapes and fast

contact detection. The mechanical interaction is characterized using the so-called soft contact approach. In this approach, although the particles are assumed to be rigid for purposes of shape definition, elastic deformation is allowed to take place at the contacts. The constitutive contact law is shown in Figure 1. It consists of two parts:

(1) a stiffness model providing a linear elastic relation between contact force and contact relative displacement in normal and shear directions; and

(2) a slip model enforcing a relation of Coulomb's type between shear and normal contact forces (Cundall and Strack, 1979).

Due to the dynamic formation of the model, energy dissipation through frictional sliding may not be sufficient to reach a steady-state solution. Additional dissipation is achieved by small amounts of viscous damping. The forces generated at a contact are computed based on the overlap of the bodies at the contact and the stiffness of the springs. The forces from all of the contacts on a single body are summed yielding a resultant force, which is then used to compute the acceleration of the body according to Newton's second law of motion. After the acceleration is determined, new velocity and displacement for the particle are computed using central difference explicit time integration. With the newly computed displacement configuration, the state of deformation at existing contacts is re-evaluated and the possible creation of new contacts is evaluated, leading to a new cycle of computation.

The parameters involved in the DEM numerical analysis include the normal stiffness k_n, normal damping ratio η_n, tangent stiffness k_s and tangent damping ratio η_s.

In this work, a biaxial shearing test is simulated using DEM. The DEM specimen consists of 3,600 circular particles (disks) of 5 and 9 mm in diameter (mixing ratio of 3:2 by area), which is generated randomly within a 42×28 cm rectangular area that is bounded by four rigid walls. The initial void ratio of the specimen is 0.1752.

The input parameters used in the simulation are listed in Table I. The stiffness k is obtained from the contact theory of two elastic discs by considering the possible stress
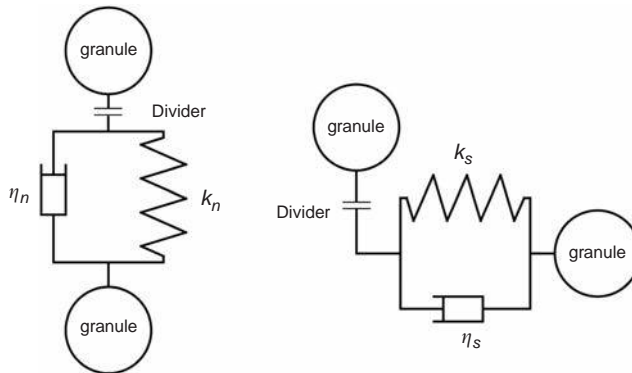
Figure 1.
DEM particle contact model

	Normal stiffness (k_n)	Tangent stiffness (k_s)	Normal damping (η_n)	Tangent damping (η_s)	Inter-particle friction angle (φ_μ)	Particle density (ρ)
Table I. Input parameters in DEM simulation	9.0×10^9 N/m^2	3.0×10^8 N/m^2	7.9×10^4 N·s/m^2	1.4×10^4 N·s/m^2	16°	2,700 kg/m^3

level applied to the granular sample (Roak, 1965), and the damping ratio η is the critical attenuation coefficient of the single degree-of-freedom system vibration. The inter-particle friction angle φ_u is obtained from the frictional tests on aluminum rods. The simulation results agreed very well with the experimental results (Liu and Lu, 2000; Liu and Xu, 2001; Liu and Sun, 2002; Liu and Matsuoka, 2003; Liu, 2006).

As shown in Figure 2, the DEM simulation is performed along the following four stress paths: isotropic compression, shearing under the condition of a constant p, shearing under the condition of a constant σ_3 and laterally confined compression (lateral displacement of the specimen is kept to be zero). Figure 3 shows the numerically simulated results in terms of the $\varepsilon_v \sim p$ relation for the isotropic and laterally confined compression paths and the $(\sigma_1 - \sigma_3) \sim \varepsilon_1 \sim \varepsilon_v$ relations for the shearing paths under a constant p and σ_3. The simulating four stress paths all start from a same initial mean stress of $p_0 = 50$ kPa. It can be seen that these numerically simulated stress-strain relationships have a regular pattern with those obtained from experiments on granular soils.

3. Microstructures of granular materials
The microstructures of granular materials change with the increase in externally applied stresses during the loading process. At present, there are several ways to characterize the microstructures of granular materials, such as fabric tensor (Satake, 1982), coordination number, comprehensive structure potential (Xie and Qi, 1999) and particle contact angles (Liu *et al.*, 2009). In our previous works, we preferred to use the particle contact angle, which is defined to be an angle of the connection line of two contacting circular particles' centers inclined to a certain base level, with a positive in counterclockwise direction, as indicated in Figure 4. Here, the base level is chosen to be the action plane of the major principal stress σ_1.

Figure 5 shows the distributions of particle contact forces under isotropic compression and shearing ($p =$ constant), respectively, in which the thickness of lines represents the magnitude of the contact forces. It is seen that there are several force chains formed by the particle contact forces. The force chains are nearly round under isotropic compression, and tend to be elliptic when the particle contact forces begin to concentrate along the direction of the major principal stress during shearing.

Denoting $F(\alpha)$ as the average of particle contact forces at the particle contact angle α, the distribution of $F(\alpha)$ in accordance with Figure 5 is shown in Figure 6. It is seen that the jagged distribution of $F(\alpha)$ can be fitted by a circle during isotropic
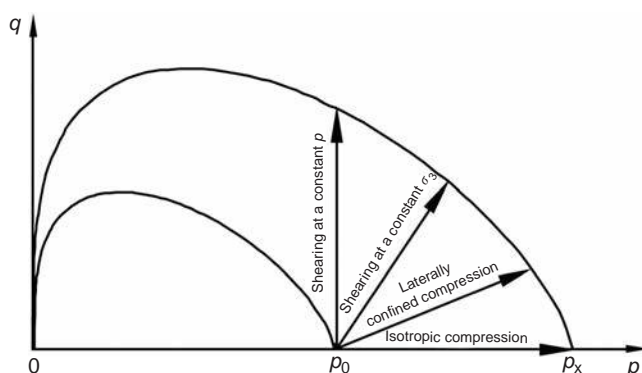
Figure 2.
Loading stress paths in the DEM simulation
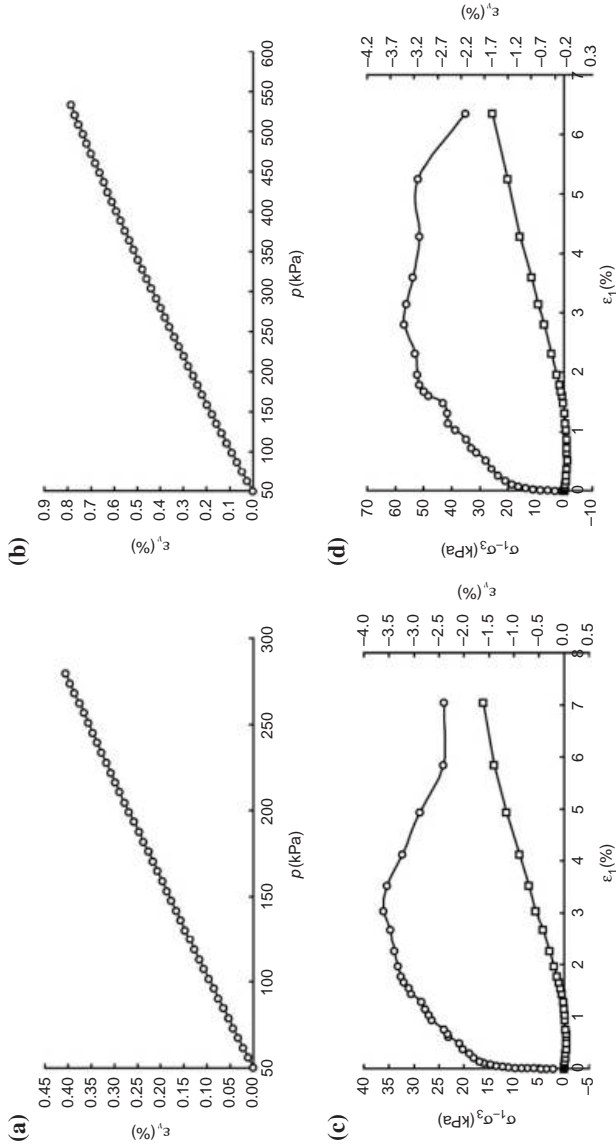
Figure 3.
Numerically
simulated
stress-strain
relationships under
four different
stress paths

Notes: (a) Isotropic compression; (b) laterally confined compression; (c) shearing under the condition of a constant p; (d) shearing under the condition of a constant σ_3
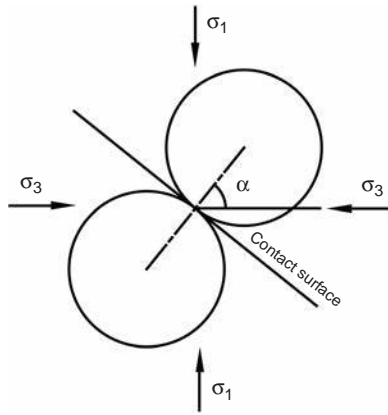
Figure 4.
Definition of particle
contact angle
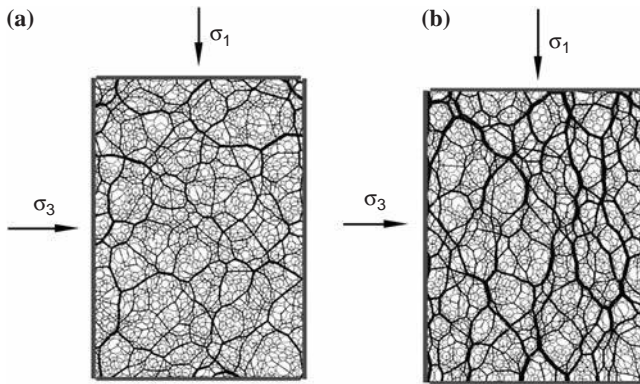
Notes: (a) Isotropic compression ($\sigma_1 = \sigma_3$); (b) shear state
($\sigma_1 > \sigma_3$)

Figure 5.
Distribution of
particle contact
forces
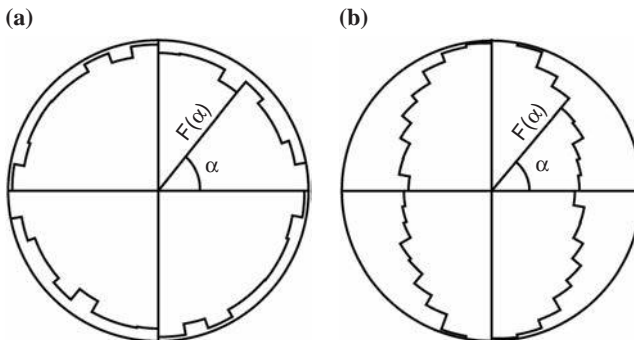
Notes: (a) Isotropic compression ($\sigma_1 = \sigma_3$); (b) shear state
($\sigma_1 > \sigma_3$)

Figure 6.
Distribution of $F(\alpha)$

compression, and it gradually changes to be elliptic during shearing, which agree well with the development of the contact force chains.

As the particle contact forces transfer through the contacting points, the concentration of the particle contact forces along the direction of the major principal stress means the increase in the number of the particle contact points along the major principal stress. Denote $\overline{N}(\alpha)$ the number of particle contact points with respect to the contact angle α, normalized by dividing the total number of the contact points at the whole sample. The distribution of $\overline{N}(\alpha)$ in accordance with Figure 5 is shown in Figure 7. Similar to the distribution of $F(\alpha)$, the jagged distribution of $\overline{N}(\alpha)$ changes from a rough circle during isotropic compression to a peanuts-like or elliptic shape during shearing.

In fact, the force chains in Figure 5 can be regarded as the microstructures of granular materials (Socolar *et al.*, 2002), which contain two components: the contact forces and the contact points. The distribution of $F(\alpha)$ characterizes the features of contact forces, whereas the distribution of $\overline{N}(\alpha)$ represents the features of the contact points (particle linkage and arrangement). Thus, a new distribution of the dot product operation $\overline{N}(\alpha) \cdot F(\alpha)$ that comprehensively considers the features of the contact forces and contact points is proposed. Figure 8 shows the distribution of $\overline{N}(\alpha) \cdot F(\alpha)$,
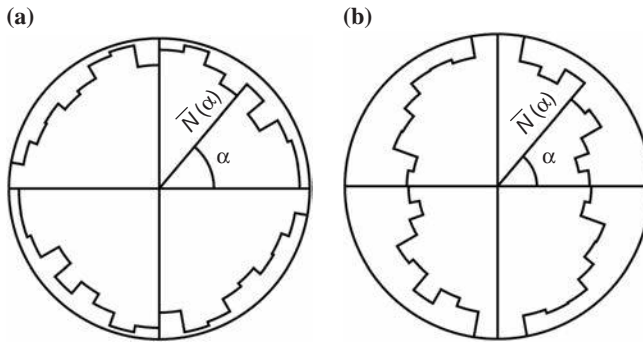
(a)　　　　**(b)**

Figure 7.
Distribution of $\overline{N}(\alpha)$

Notes: (a) Isotropic compression ($\sigma_1 = \sigma_3$); (b) shear state ($\sigma_1 > \sigma_3$)

(a)　　　　**(b)**

Figure 8.
Distribution of $\overline{N}(\alpha) \cdot F(\alpha)$

Notes: (a) Isotropic compression ($\sigma_1 = \sigma_3$); (b) shear state ($\sigma_1 > \sigma_3$)

combining with Figures 6 and 7. The new distribution of $\overline{N}(\alpha)\cdot F(\alpha)$ has the same characteristic as the distribution of either $F(\alpha)$ or $\overline{N}(\alpha)$, i.e. the isotropy of the microstructures maintains during isotropic compression and the anisotropy develops during shearing.

The proposed distribution of $\overline{N}(\alpha)\cdot F(\alpha)$ reflects the microstructures of the sample at a certain stress state, which will change during the loading process. In order to quantitatively characterize the change of the microstructures, a parameter S is suggested, which is defined as:

$$\text{S} = \left|\overline{N}(\alpha)\cdot F(\alpha)\right| = \sqrt{\sum\left(\overline{N}(\alpha)\cdot F(\alpha)\right)^2} \tag{1}$$

Figure 9 shows the evolution of the parameter S during the loading process under the four different stress paths, in which the macro stress-strain relationships are given as well. It is seen that the evolution of the parameter S matches well with that of the macro stresses during the loading process. As the macro-mechanical behavior of granular materials is inherently related to their microstructures, the results shown in Figure 9 demonstrate the reasonability of the parameter S suggested.

Figure 10 gives the distributions of $\overline{N}(\alpha)\cdot F(\alpha)$ at the points A and B in Figures 9(d), respectively. The point A corresponds to a high level of stress with a high value of S, and the point B represents the stress state after the failure with a decreasing S. It is seen from Figure 10(b) that the $\overline{N}(\alpha)\cdot F(\alpha)$ decreases roughly in the range of the contact angle $\alpha = 35\sim55°$ and $215\sim235°$, leading to the decrease of S value at point B. For this sample, the internal friction angle φ is calculated to be $20°$. Normally, the shear band is inclined to the action plane of the major principal stress σ_1 with an angle of $45°+ \varnothing/2 = 55°$. Within the shear band, some particle contacts disappear and the contact forces decrease. The decrease of $\overline{N}(\alpha)\cdot F(\alpha)$ at point B falls roughly within the shear band.

4. Yield function derived from microstructures
Most of the yield functions of the existing elastic-plastic constitutive models for soils have been obtained macroscopically from laboratory triaxial compression tests. For example, Cam-clay model (Roscoe *et al.*, 1963; Roscoe and Burland, 1968) was based on the results of triaxial compression tests on normally consolidated clays, in which an experimentally obtained stress-dilatancy relationship was used and plastic volumetric strain is taken as hardening parameter. To our knowledge, few attentions have been paid on the microscopic essence of yield functions. As the yielding of granular materials is inevitably accompanied with the change of the microstructures of particles (Matsuoka *et al.*, 1995), and the parameter S proposed in this paper can characterize the microstructures, it is thus possible to use the parameter S as a hardening parameter to describe the yielding of granular materials. The numerical results in Figure 9 indicate that the parameter S changes during compression and shearing, namely, it is directly affected by stress states. Therefore, the parameter S is an internal variable that reflects the changing degree of granular material microstructures after the application of external stresses, and may be used as a hardening parameter to quantitatively describe the yielding of granular materials.

As stated above, four different stress paths starting from the same mean stress $p = 50\,\text{kPa}$ have been numerically simulated in this work. First, we consider the changes of the parameter S along two stress paths: one is the isotropic compression
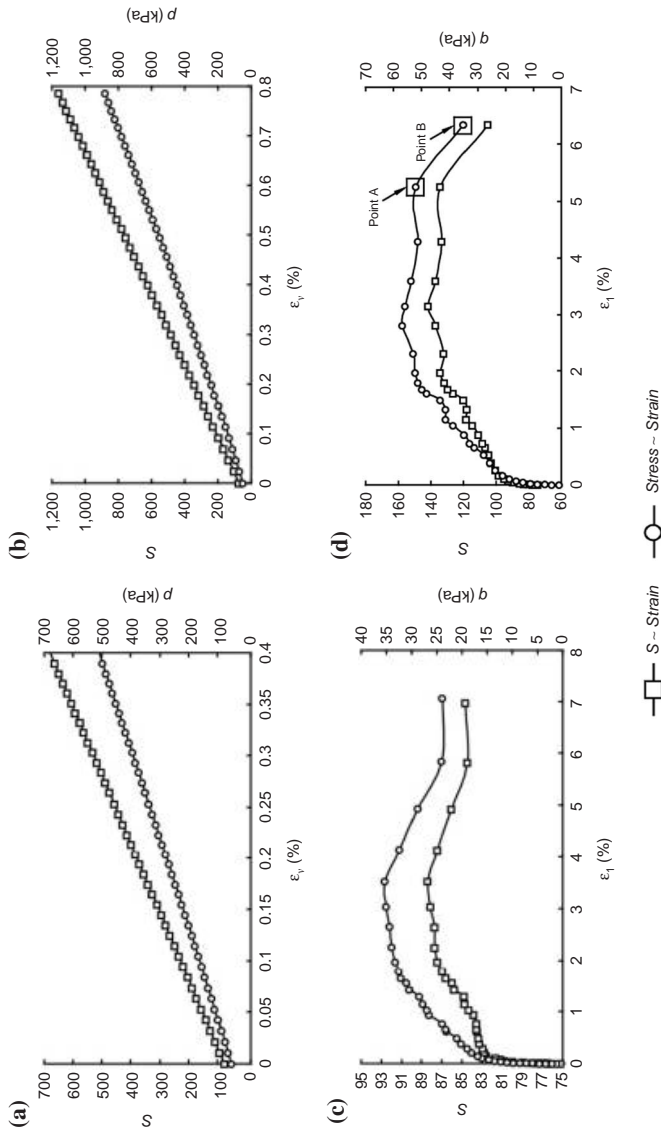
Figure 9.
Evolution of
microstructure
parameter S and
macro stress during
loading along four
different stress paths

Notes: (a) Isotropic compression; (b) laterally confined compression; (c) shearing under the condition of a constant p;
(d) shearing under the condition of a constant σ_3

path, and the other is the shearing path at a constant p (cf. Figure 2). Figures 11 and 12 give the changes of the microstructure parameter S plotted against the externally applied macro stresses along these two stress paths, respectively. Both of them can be fitted in the form of an exponential function, expressed as:

$$\frac{\Delta S_p}{\Delta S} = 0.939 \left(\frac{p_x - p}{p} \right)^{0.978} \quad (2)$$
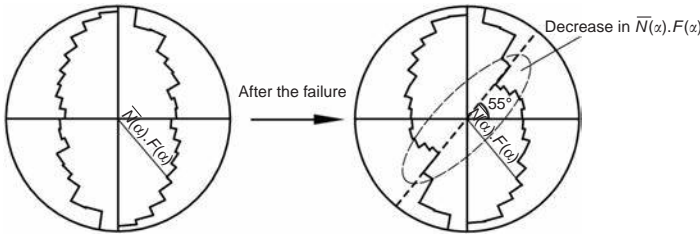
Notes: (a) At point A; (b) at point B

Figure 10.
Distribution of $\overline{N}(\alpha) \cdot F(\alpha)$ at the points A and B
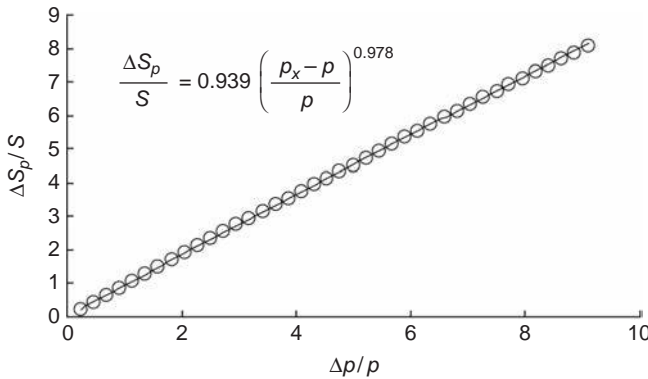
Figure 11.
Changes of the microstructure parameter S against the macro stress during isotropic compression
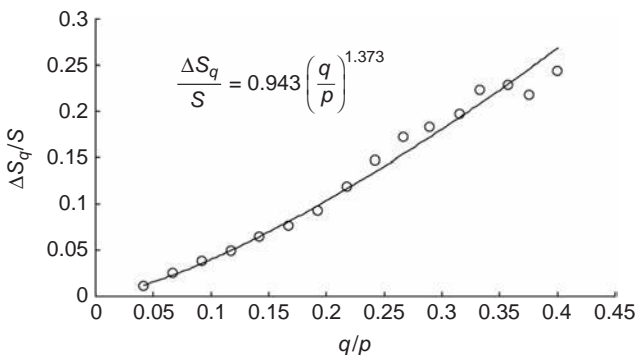
Figure 12.
Change of the microstructure parameter S against the macro stress during shearing at $p = 50\,kPa$

$$\frac{\Delta S_q}{S} = 0.943 \left(\frac{q}{p}\right)^{1.373} \tag{3}$$

where p is the initial mean stress (50 kPa); S is the microstructure parameter at $p = 50$ kPa; p_x and q are the mean stress and the deviator stress during loading, respectively; ΔS_p and ΔS_q are the increments of the microstructure parameter S during isotropic compression and shearing at a constant p with respect to the initial stress state, respectively.

As the microstructure parameter S is taken as the hardening parameter that is the same on a yield surface, we can get:

$$\Delta S_p = \Delta S_q \tag{4}$$

Consequently, from Equations (2) and (3), we can obtain a yield function of granular materials based on the microstructures, which is expressed as:

$$f = k_2 \left(\frac{q}{p}\right)^{n_2} - k_1 \left(\frac{p_x}{p}-1\right)^{n_1} = 0 \tag{5}$$

where k_1 and n_1 are the coefficient and index related to isotropic compression, respectively, while k_2 and n_2 are the coefficient and index related to the shearing under the condition of a constant p, respectively. Equation (5) can be rewritten as:

$$f = \frac{q}{p} - k \left(\frac{p_x}{p}-1\right)^{n} = 0 \tag{6}$$

where $n = n_1/n_2$, $k = (k_1/k_2)^{1/n_2}$. For the simulated sample, $k_1 = 0.939$, $k_2 = 0.943$, $n_1 = 0.978$, $n_2 = 1.373$, $k = 0.997$, $n = 0.712$.

Similarly, we can get a yield function from the changes of the microstructure parameter S along another two simulating stress paths, i.e. laterally confined compression and shearing at a constant σ_3 (cf. Figure 2). Figures 13 and 14 give respectively the relevant changes of the microstructure parameter S, together with the fitting expressions. The yield function derived from the changes of the microstructures along these two stress paths is:

$$f = \frac{q}{p} - 0.951 \left(\frac{p_x}{p}-1\right)^{0.733} = 0 \tag{7}$$
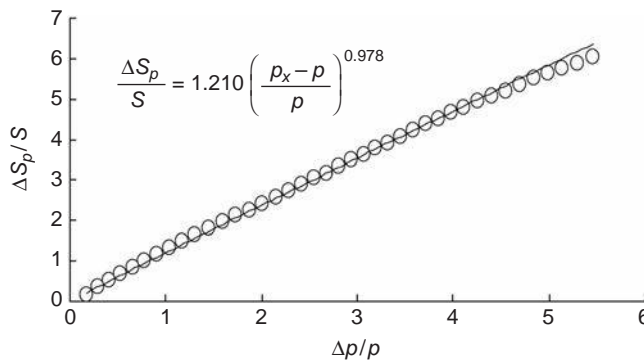
Figure 13.
Change of the microstructure parameter S against the macro stress during laterally confined compression

Figure 15 shows the yield curves drawn from Equations (6) and (7). It can be seen that the two curves agree very closely, illustrating that the changes of the microstructure parameter S along different stress paths starting from the same initial stress state are the same on a yield surface. Thus, it is rational to take the proposed microstructure parameter S as a hardening parameter in the derivation of the yield function for granular materials.

5. Validation of the derived yield functions
5.1 Determination of the yield function's parameters
A yield function of granular materials is derived from the variation of the microstructure parameter S in this paper, in which two parameters (n and k) are involved. Although the two parameters depend on the microstructures, they should also be related to the macro behaviors of granular materials. It is thus possible to determine these two parameters from macro experiments, which is helpful to the application of the derived yield function.

The microstructure parameter S is obtained from the dot product of the distributions of both contact forces and particle arrangements, which are related to the mechanical behavior and deformation of granular materials, respectively. Therefore, the microstructure parameter S is equivalent to energy at a macro-level.

$$\frac{\Delta S_q}{S} = 1.294 \left(\frac{q}{p} \right)^{1.335}$$
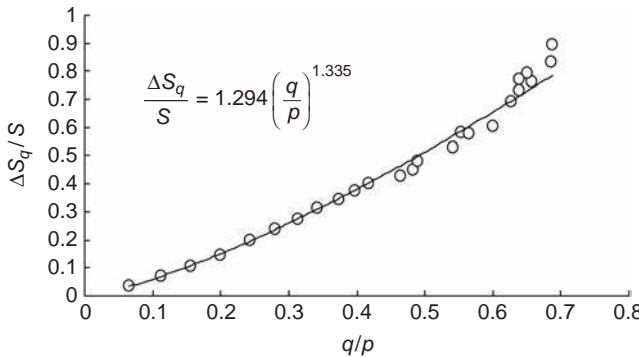
Figure 14.
Change of the microstructure parameter S against the macro stress during shearing at a constant σ_3

From the stress paths of isotropic compression and shearing at a constant p

From the stress paths of laterally confined compression and shearing at a constant σ_3
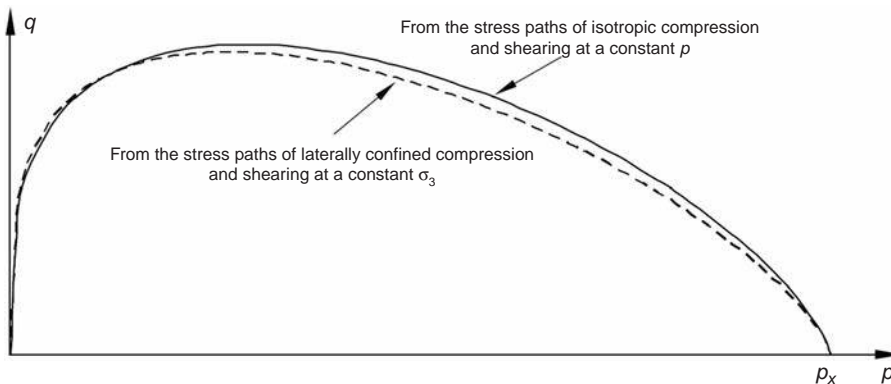
Figure 15.
Microstructure-based yield surfaces of granular materials from different stress paths

As mentioned above, the yield function in this paper is derived on the assumption that the changes of the microstructure parameter S are the same whatever the loading stress paths are from the same initial stress state to a new yield surface. Based on the same assumption, the two parameters involved in the yield function can be determined from the energy changes that are obtained from macro experiments. The energy change is calculated to be for compression paths and for shearing paths, where and are the increments of volumetric strain and deviator stain, respectively.

5.2 Validation by tests on one sand

Both the isotropic compression and the triaxial compression tests are conducted on one sand, which has a grain diameter of 0.176~1.982 mm, a uniformity coefficient of $C_u = 2.387$, a curvature coefficient of $C_c = 0.905$ and a specific weight of $G_s = 2.67$. The density of the prepared specimen is 2.1 g/cm^3. Starting from the initial stress state of $\sigma_1 = \sigma_3 = 100$ kPa, the isotropic compression test is carried out by increasing simultaneously σ_1 and σ_3, while the triaxial compression test is carried out by increasing σ_1 under the constant $\sigma_3 = 100$ kPa. Figure 16 gives the stress-strain relations of these two tests, from which the energy changes can be calculated. Figures 17 and 18 show the calculated energy changes against the macro stress during the isotropic and triaxial compressions, respectively, which can be fitted by a power exponent equation.
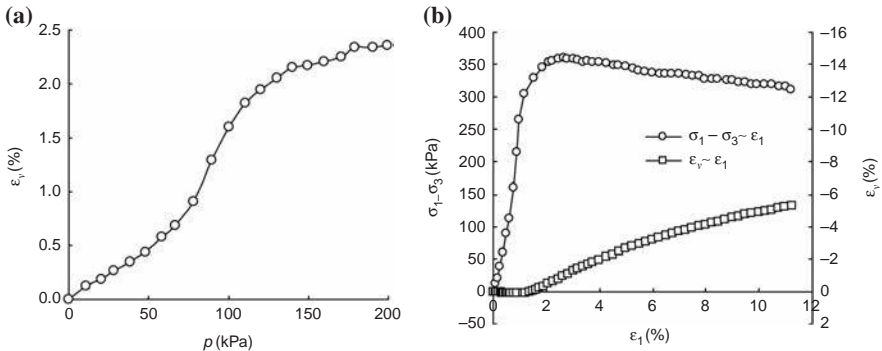
Figure 16.
Stress-strain relationships of the tested sand from isotropic and triaxial compressions

Notes: (a) Isotropic compression; (b) triaxial compression
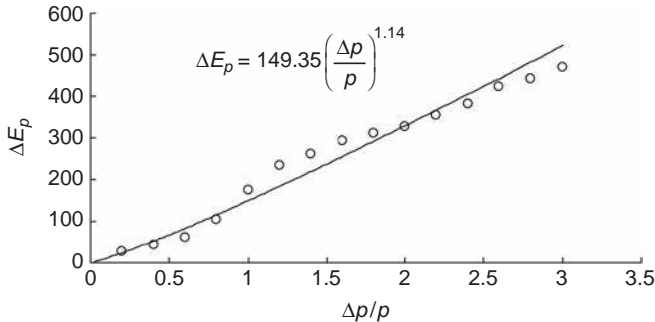
Figure 17.
Energy change against the macro stress during isotropic compression

$$\Delta E_p = 149.35 \left(\frac{\Delta p}{p} \right)^{1.14}$$

As stated above, $\Delta Ep = \Delta Eq$ when the samples yield. From the fitting equations as shown in Figures 17 and 18, the parameters involved in Equations (5) and (6) are determined as: $k_1 = 149.35$, $k_2 = 96.38$, $n_1 = 1.14$, $n_2 = 1.63$, $k = 1.31$, $n = 0.70$. Finally, the yield function of the tested sand is expressed as:

$$f = \frac{q}{p} - 1.31 \left(\frac{p_x}{p} - 1\right)^{0.70} = 0 \tag{8}$$

Figure 19 shows the yield surface drawn from Equation (8). For the comparison, the yield surfaces of both the original and modified Cam-clay models, expressed as Equations (9) and (10), are also shown in Figure 19.

The original Cam-clay model:

$$f = \frac{q}{p} - Mln\frac{p_x}{p} = 0 \tag{9}$$

The modified Cam-clay model:

$$f = q^2 + M^2\left(p^2 - p_x\,p\right) = 0 \tag{10}$$

In Figure 19, the parameter M used in the Cam-clay models is taken as 1.64, which is calculated from $6\,sin\varphi/(3 - sin\varphi)$ with φ 40° (cf. Figure 16(b)). It can be seen that the yield surface based on the changes of the microstructures is similar to those of the Cam-clay
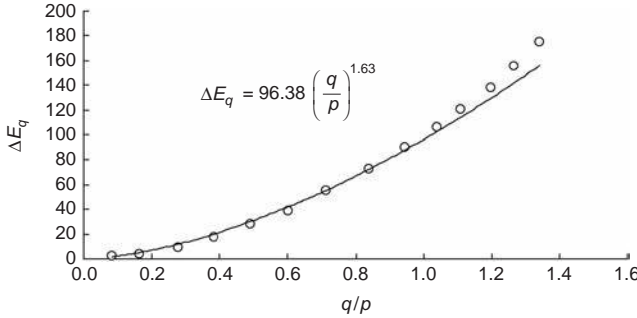
Figure 18.
Energy change against the macro stress during triaxial compression
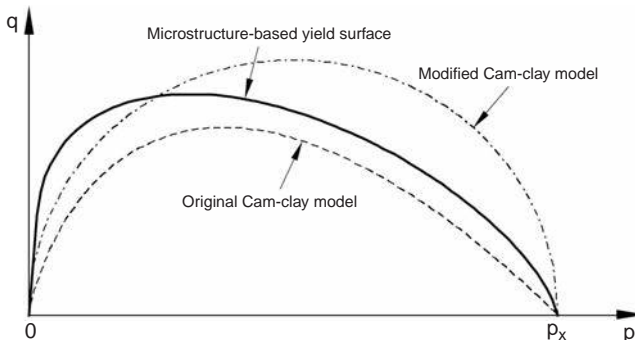
Figure 19.
Yield surfaces of the tested sand

models, and is located between them. Equation (10) of the modified Cam-clay model is re-arranged as:

$$f = \frac{q}{p} - M\left(\frac{p_x}{p} - 1\right)^{0.5} = 0 \tag{10}$$

Thus, the yield function proposed in this paper has a same form as the modified Cam-clay model with $k = M$ and $n = 0.5$. In Figure 19, the yield surface changes with the mean stress p_x. In the Cam-clay models, p_x is related to the plastic volumetric strain, namely, the hardening parameter is the plastic volumetric strain. In fact, plastic volumetric strain is directly relevant to void ratio e, which represents the particles' geometric arrangement and reflects particles' microstructures. Thus, the hardening parameter of plastic volumetric strain in the Cam-clay models indirectly reflects the changes of particle microstructures. In the establishment of the Cam-clay model, the energy dissipation equation of $pd\varepsilon_v^p + qd\varepsilon_d^p = Mpd\varepsilon_d^p$ is used, i.e., the energy produced during the loading process is equal to the energy at failure. Obviously, this is only an assumption and conflicts with the reality. However, this drawback does not exist in the derivation of the microstructure-based yield function in this paper.

5.3 Validation by using test data of two rockfill materials

Furthermore, the proposed yield functions are analyzed using the test data of two rockfill materials (named as SJ1 and SJ2), which were taken from a hydropower station construction site. Figures 20 and 21 give the test results of the two rockfill materials, respectively, in which the e-p curves were obtained from the laterally confined compression tests with a specimen diameter of 45 cm and the stress-strain curves were obtained from large-scale triaxial compression tests (the specimen diameter is 30 cm).

As the yield function proposed in this paper is based on the same changes of the microstructures or energy from the same initial stress state to the yield surface, the analysis for the energy changes in the triaxial compression tests and the laterally confined compression tests should start from the same initial stress state. For the
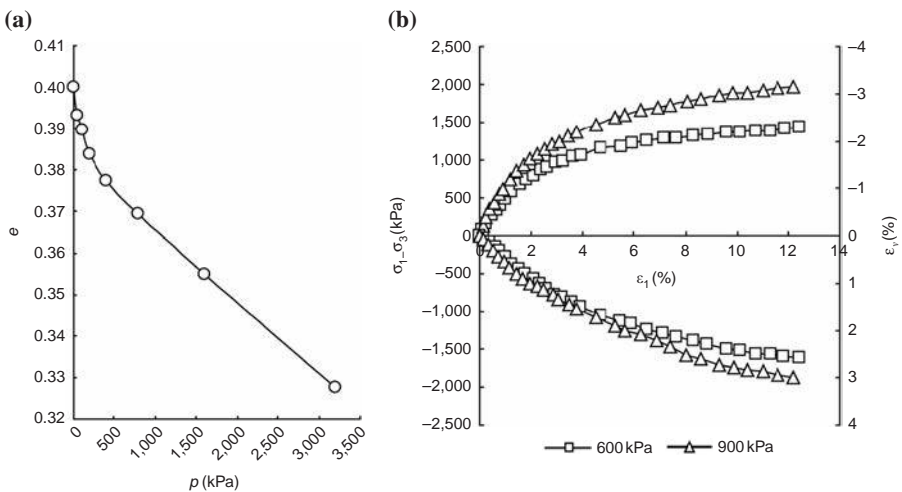
Figure 20.
Results of
(a) laterally confined
compression test and
(b) triaxial
compression
test on SJ1
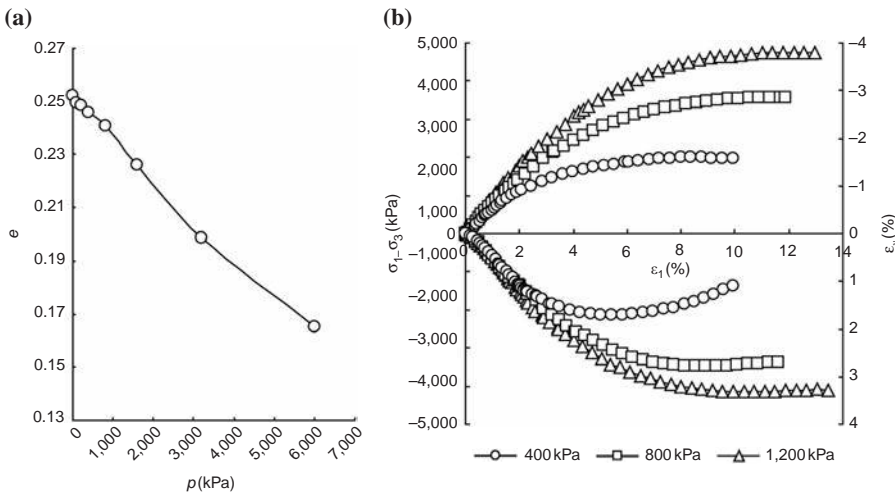
Figure 21.
Results of
(a) laterally confined
compression test and
(b) triaxial
compression test
on SJ2

sample SJ1, the triaxial compression tests were carried out under the confining stresses $\sigma_3 = 600$ and 900 kPa, which correspond to the initial void ratio $e_0 = 0.373$ and 0.367 in the laterally confined compression tests, respectively (cf. Figure 20). Figure 22 gives the energy changes of the sample SJ1 in the triaxial and laterally confined compression tests in accordance with the two initial stress states, calculated using the test data in Figure 20. Similarly, Figure 23 gives the energy changes of the sample SJ2 in the triaxial and laterally confined compression tests in accordance with three initial stress states of $\sigma_3 = 400$, 800 and 1,200 kPa (respectively corresponding to the initial void ratios of 0.246, 0.241 and 0.234), calculated using the test data in Figure 21.

The yield functions established from the energy changes in Figures 22 and 23 are listed in Table II, and the corresponding yield surfaces are shown in Figure 24. The frictional angles of the samples SJ1 and SJ2 obtained from the triaxial compression
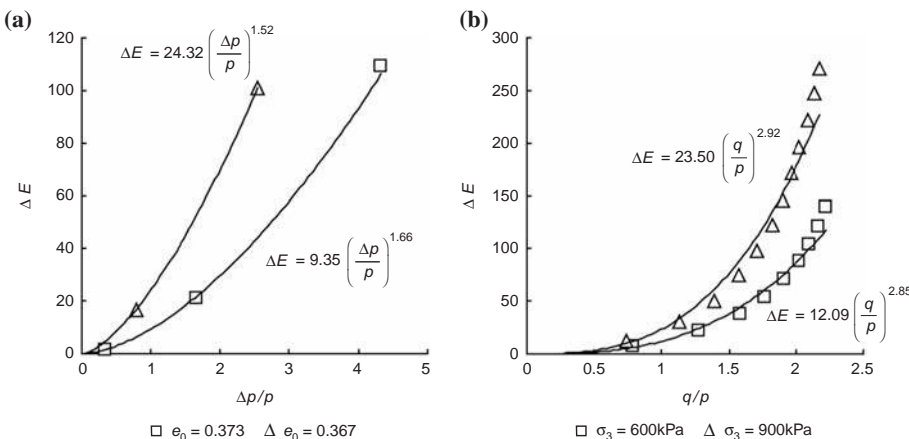
Notes: (a) Laterally confined test; (b) triaxial compression test

Figure 22.
Energy changes of
the sample SJ1
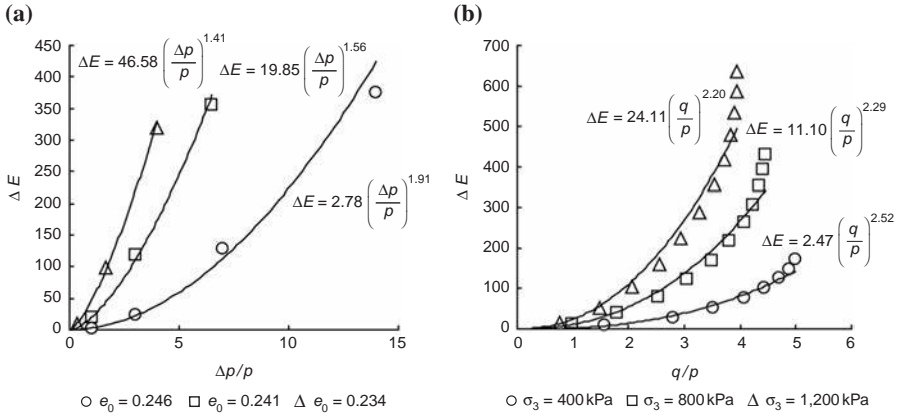
Figure 23.
Energy changes of
the sample SJ2

Notes: (a) Laterally confined test; (b) triaxial compression test

Initial confining stresses/initial void ratio	SJ1	Initial confining stresses/initial void ratio	SJ2
600 kPa/0.373	$f = \frac{q}{p} - 0.91\left(\frac{p_x}{p}-1\right)^{0.58} = 0$	400 kPa/0.246	$f = \frac{q}{p} - 1.05\left(\frac{p_x}{p}-1\right)^{0.76} = 0$
900 kPa/0.367	$f = \frac{q}{p} - 1.01\left(\frac{p_x}{p}-1\right)^{0.52} = 0$	800 kPa/0.241	$f = \frac{q}{p} - 1.29\left(\frac{p_x}{p}-1\right)^{0.68} = 0$
		1,200 kPa/0.234	$f = \frac{q}{p} - 1.35\left(\frac{p_x}{p}-1\right)^{0.64} = 0$
Original Cam-clay model	$f = \frac{q}{p} - 1.24\, ln\frac{p_x}{p} = 0$	Original Cam-clay model	$f = \frac{q}{p} - 1.47\, ln\frac{p_x}{p} = 0$
Modified Cam-clay model	$f = \frac{q}{p} - 1.24\left(\frac{p_x}{p}-1\right)^{0.5} = 0$	Modified Cam-clay model	$f = \frac{q}{p} - 1.47\left(\frac{p_x}{p}-1\right)^{0.5} = 0$

Table II.
Yield functions of
the two rockfill
materials established
from the energy
changes
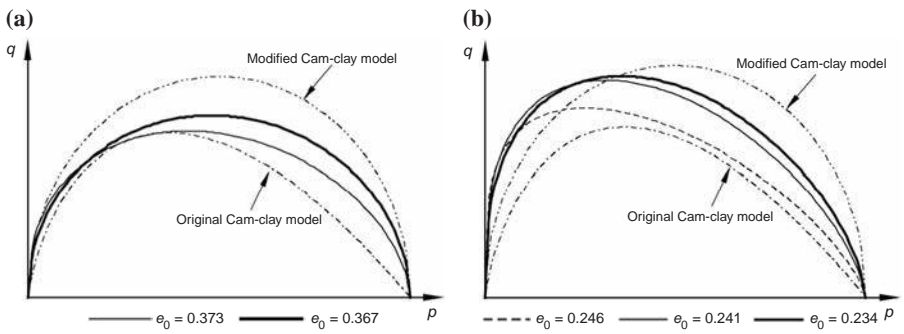
Figure 24.
Yield surfaces
obtained from the
test data of two
rockfill materials

Notes: (a) SJ1; (b) SJ2

tests are 31.0 and 36.2°, respectively, on which the yield surfaces of the Cam-clay
models are also shown in Figure 24. It is seen from Figure 24 that the shape of the yield
surface proposed in this paper is similar to those of the Cam-clay models for the two
rockfill materials as well. It can also be seen that the shape of the proposed yield surface

is influenced by the initial void ratio of the samples. The smaller the initial void ratio is, the closer the shape is to that of the modified Cam-clay. With the decrease in the initial void ratio of the sample, the parameter k in the proposed yield function increases with a maximum value of M, and the parameter n decreases with a minimum value of 0.5, where M and 0.5 are the corresponding parameters in the modified Cam-clay model.

6. Conclusions

In this work, a biaxial compression test on granular materials is numerically simulated by DEM and the variation of microstructure of granular materials under different stress paths is analyzed, from which a yield function is derived. The determination of the two parameters in the derived yield function is also studied. The proposed yield function is calibrated by the test data of one sand and two rockfill materials. The main points that can be concluded in this work are as follows:

(1) A parameter S is proposed to characterize the microstructure of granular materials, which considers comprehensively the contact forces and the linkage as well as the arrangement of granular particles. The numerical results indicate that the evolution of the proposed microstructure parameter S during different loading stress paths agrees well with the development of the macro stress and strain.

(2) It is considered that along different loading paths, the change of microstructures of granular materials from the same initial stress state to a yield surface is the same, on which a yield function is derived. There are two parameters (k and n) involved in the derived yield function, which can be determined by laboratory tests through the analysis of energy change during loading process.

(3) The calibration through the test data of one sand and two rockfill materials indicates that the shape of the new yield function is similar to that of the Cam-clay models, and is influenced by the initial void ratio of the samples. The smaller the initial void ratio of the sample is, the closer the shape of the new yield function is to that of the modified Cam-clay model.

In this study, the rolling resistance was not considered in the contact model of particles and a special particle packing with two different particle diameters was used in the numerical simulation. Further study will cover the rolling resistance and a continuously distributed specimen of grain assembly will be used to validate the rationality of the derived yield function in the future.

References

Chen, H. and Liu, S.H. (2007), "Slope failure characteristics and stabilization methods", *Canad Geotech J*, Vol. 44 No. 4, pp. 377-391.

Cundall, P.A. and Strack, O.D.L. (1979), "A discrete numerical model for granular assemblies", *Geotechnique*, Vol. 29 No. 1, pp. 47-56.

Drucker, D.C., Gibson, R.E. and Henkek, D.J. (1955), "Soil mechanics and work hardening theories of plasticity", *Journal of the Soil Mechanics and Foundation Division*, Vol. 81 No. 1, pp. 1-14.

Lade, P.V. and Duncan, J.M. (1977), "Elasto-plastic stress-strain theory for cohesionless soil with curved yield surface", *International Journal of Solids and Structures*, Vol. 13 No. 1, pp. 1019-1035.

Liu, S.H. (2006), "Simulating direct shear test by DEM", *Canad Geotech J*, Vol. 43 No. 2, pp. 155-168.

Liu, S.H. and Bauer, E. (2007), "A microscopic study of rainfall-induced granular slope failure", *Proceedings of 3rd Asian Conference on Unsaturated Soils, Nanjing*, pp. 379-383.

Liu, S.H. and Lu, T.H. (2000), "Microscopic shear mechanism of granular materials in simple shear by DEM", *Chinese J Geotech Eng*, Vol. 22 No. 5, pp. 608-611 (in Chinese).

Liu, S.H. and Matsuoka, H. (2003), "Microscopic interpretation on a stress-dilatancy relationship of granular materials", *Soils Found*, Vol. 43 No. 3, pp. 73-84.

Liu, S.H. and Sun, D.A. (2002), "Simulating the collapse of unsaturated soil by DEM", *Intern J Numer Anal Meth Geomech*, Vol. 26 No. 6, pp. 633-646.

Liu, S.H. and Xu, Y.F. (2001), "Numerical simulation for a direct box shear test on granular material and microscopic consideration", *Chinese J Rock Mech Eng*, Vol. 20 No. 3, pp. 288-292 (in Chinese).

Liu, S.H., Sun, D.A. and Wang, Y.S. (2003), "Numerical study of soil collapse behaviors by discrete element modeling", *Comput Geotech*, Vol. 30 No. 5, pp. 399-408.

Liu, S.H., Yao, Y.P., Sun, Q.C., Li, T.J. and Liu, M.Z. (2009), "Microscopic study on stress-strain relation of granular materials", *Chinese Science Bulletin*, Vol. 54 No. 23, pp. 4349-4357.

Matsuoka, H. (1974), "A microscopic study on shear mechanism of granular materials", *Soils Found*, Vol. 14 No. 1, pp. 29-43.

Matsuoka, H., Akashi, Y. and Itoh, K. (1995), "Deformation of yield surface based on fabric of granular material and its experimental check", *Proceedings of the 30th Japan National Conference on Soil Mechanics and Foundations Engineering*, pp. 579-582.

Matsuoka, H., Yao, Y.P. and Sun, D.A. (1999), "The Cam-clay models revised by the SMP criterion", *Soils and Foundations*, Vol. 39 No. 1, pp. 81-95.

Oda, M. (1972), "Initial fabrics and their relations to mechanical properties of granular material", *Soils Found*, Vol. 12 No. 1, pp. 17-36.

Roak, R.J. (1965), *Formulas for Stress and Strain*, 4th ed., McGraw-Hill, New York, NY, pp. 319-321.

Roscoe, K.H. and Burland, J.B. (1968), "On the generalized stress-strain behavior of 'wet' clay", in Heyman, J. and Leckie, F.A. (Eds), *Engineering Plasticity*, Cambridge University Press, Cambridge, pp. 535-609.

Roscoe, K.H., Schofield, A.N. and Thurairajah, A. (1963), "Yielding of clay in states wetter than critical", *Geotechnique*, Vol. 13 No. 3, pp. 221-240.

Roscoe, K.H., Schofield, A.N. and Wroth, C.P. (1958), "On the yielding of soils", *Geotechnique*, Vol. 8 No. 1, pp. 22-53.

Satake, M. (1982), "Fabric tensor in granular materials", *IUTAM Conference on Deformation and Flow of Granular Materials*, pp. 63-68.

Socolar, J.E.S., Schaeffer, D.G. and Claudin, P. (2002), "Directed force chain networks and stress response in static granular materials", *The European Physical Journal E*, Vol. 7 No. 4, pp. 353-370.

Xie, D.Y. and Qi, J.L. (1999), "Soil structure characteristics and new approach in research on its quantitative parameter", *Chinese Journal of Geotechnical Engineering*, Vol. 21 No. 6, pp. 651-656.

Corresponding author

Zijian Wang can be contacted at: wwzzjj618@163.com